INTERNATIONAL JOURNAL FOR NUMERICAL METHODS IN FLUIDS
Int. J. Numer. Meth. Fluids **30**: 407–424 (1999)

A PARTICLE–GRIDLESS HYBRID METHOD FOR INCOMPRESSIBLE FLOWS

HAN YOUNG YOON*, SEIICHI KOSHIZUKA AND YOSHIAKI OKA

Nuclear Engineering Research Laboratory, Faculty of Engineering, The University of Tokyo, 2-22 Shirane, Shirakata, Tokai-mura, Naka-gun, Ibaraki 319-11, Japan

SUMMARY

A particle–gridless hybrid method for the analysis of incompressible flows is presented. The numerical scheme consists of Lagrangian and Eulerian phases as in an arbitrary Lagrangian–Eulerian (ALE) method, where a new-time physical property at an arbitrary position is determined by introducing an artificial velocity. For the Lagrangian calculation, the moving-particle semi-implicit (MPS) method is used. Diffusion and pressure gradient terms of the Navier–Stokes equation are calculated using the particle interaction models of the MPS method. As an incompressible condition, divergence of velocity is used while the particle number density is kept constant in the MPS method. For the Eulerian calculation, an accurate and stable convection scheme is developed. This convection scheme is based on a flow directional local grid so that it can be applied to multi-dimensional convection problems easily. A two-dimensional pure convection problem is calculated and a more accurate and stable solution is obtained compared with other schemes. The particle–gridless hybrid method is applied to the analysis of sloshing problems. The amplitude and period of sloshing are predicted accurately by the present method. The range of the occurrence of self-induced sloshing predicted by the present method shows good agreement with the experimental data. Calculations have succeeded even for the higher injection velocity range, where the grid method fails to simulate. Copyright © 1999 John Wiley & Sons, Ltd.

KEY WORDS: particle–gridless hybrid; gridless method; MPS; flow directional local grid; incompressibility; free-surface; sloshing

1. INTRODUCTION

Computer simulation has been required to analyse increasingly complex geometry and physics problems. However, there are still many thermal-hydraulic problems that are difficult to analyse with conventional grid methods, such as finite difference or finite element methods. Recently, numerical methods that do not use any grid structure were developed for the application to the analyses of thermal-hydraulic problems having complex geometries and interfaces where the conventional grid methods suffer from mesh generation. These meshless methods can be roughly classified into two groups: (1) those based on Lagrangian (particle) methods, such as smoothed particle hydrodynamics (SPH) [1,2] and moving-particle semi-implicit (MPS) [3,4] and (2) those based on Eulerian (gridless) methods, such as a gridless Euler/Navier–Stokes solution algorithm [5] and element free Galerkin (EFG) [6].

* Correspondence to: Nuclear Engineering Research Laboratory, Faculty of Engineering, The University of Tokyo, 2-22 Shirane, Shirakata, Tokai-mura, Ibaraki Prefective 319-11, Japan.

CCC 0271–2091/99/120407–18$17.50

Received December 1997
Revised April 1998

In particle methods, each particle moves in Lagrangian co-ordinates and convection is directly calculated by the motion of particles without numerical diffusion. SPH has been used in astrophysics to determine the fluid dynamics of interstellar gas, which is regarded as a compressible invicid fluid. The MPS method has been developed for the application to incompressible viscous flow. In the MPS method, the motion of each particle is calculated through interactions with neighbouring particles covered with a weight function. All terms in the Navier–Stokes equation, such as gradient and Laplacian terms are represented by the deterministic particle interaction models. Pressure is calculated implicitly by using the incompressibility condition of constant particle number density. Dam breaking [3,7] and vapour explosion [4,8] were calculated with fluid fragmentation using the MPS method. As long as a problem can be described in Lagrangian co-ordinates, many complicated problems can be calculated easily by the MPS method. In many situations, however, there exists inflow or outflow making it difficult to trace a particle in Lagrangian co-ordinates.

As an Eulerian approach, Batina has introduced a gridless method for the solution of Navier–Stokes equation. In this method, a physical property is interpolated linearly based on the least-squares and the spatial derivatives in the governing equations are found to be the coefficients of the linear function. Thus, it allows the use of fields of points where the points are more appropriately located and clustered, which makes it easier to apply to complex geometry than the grid methods. Although this method can be applied easily to arbitrary clouds of points, a large amount of numerical diffusion is inevitable during the calculation of convection and the artificial dissipation must be added explicitly to the solution procedure.

A less diffusive numerical algorithm, cubic interpolation in area co-ordinates with a triangular unit (CAT) [9], was proposed based on the CIP [10] in two dimensions. The accuracy of the gridless method was markedly improved by introducing a higher-order interpolation scheme. In this method, a particle moves in Lagrangian co-ordinates and goes back to its original position using the CIP interpolation in one time step. In general, a particle does not need to go back to its original position and can be placed freely. This concept corresponds to the arbitrary Lagrangian–Eulerian (ALE) method [11], where a new-time property at an arbitrary position is determined by introducing artificial velocities. It is essential in this method, to construct well-defined triangles out of arbitrarily distributed particles since all the calculations are carried out in area co-ordinates with triangular units. Sometimes, however, construction of a well-defined triangle is troublesome, especially when the computing points are scattered at random. In three dimensions, making a tetrahedron from random points is a laborious task.

In this paper an accurate and stable gridless method that can be applied to multi-dimensional convection problems is proposed based on a flow directional local grid. This numerical scheme consists of four stages: (1) a one-dimensional local grid is generated in the flow direction of each particle, (2) physical properties of the local grid points are interpolated using a weight function, (3) a higher-order convection scheme is applied to the one-dimensional local grid and (4) a filtering scheme MMT [12] is applied to get a stable solution. Utilisation of a weight function used in the MPS method makes this scheme completely free from grid structure. Numerical diffusion occurring during the interpolation is kept small by applying a higher-order difference scheme to the flow directional local grid. Propagation of a two-dimensional square wave is simulated using the present method and the results are compared with the previous gridless schemes for both uniform and random particle distributions.

Combining the present gridless method with the MPS method, a particle–gridless hybrid method is proposed for the analysis of incompressible flows having inlet or outlet boundaries. In the MPS method, the particle number density is kept constant as the incompressible

condition because the particle number density is proportional to the fluid density. The pressure is calculated by solving the pressure Poisson equation where the deviation of the particle number density is used as a source term. However, the incompressibility model using the particle number density can not be applied to the present study because the particle number density does not change in Eulerian co-ordinates. Instead, a new incompressibility model where the velocity divergence is calculated using a weight function is proposed.

Sloshing problems induced by an external pressure spike and an internal flow are calculated using the present method. Since the boundary condition at the free-surface is non-linear, the flow with free-surfaces is complex and sometimes not unique. Several numerical simulation methods had been proposed to predict the flow with free-surfaces. In the marker and cell method (MAC) [13] and the volume of fluid method (VOF) [14], the free-surface was tracked with the fixed grid system. The free-surface location was determined by the distribution of the markers and the volume of fluid in each cell respectively. In the boundary fitted co-ordinate method (BFC) [15,16], the free-surface was tracked with Lagrangian–Eulerian flexible grids. These methods could simulate relatively small displacement of free-surface. When the velocity under the free-surface or the amplitude of the wave increases, large deformation of the free-surface occurs, causing the simulation to be difficult. These difficulties are overcome by the present method since a large deformation of the free-surfaces can be analysed using the particle interaction models of the MPS method [3,7].

2. GOVERNING EQUATIONS

Governing equations for incompressible flows are the continuity and the Navier–Stokes equations as follows:

$$\nabla \cdot \mathbf{u} = 0, \tag{1}$$

$$\frac{\partial \mathbf{u}}{\partial t} + \mathbf{u} \cdot \nabla \mathbf{u} = -\frac{1}{\rho} \nabla P + \nu \nabla^2 \mathbf{u} + \mathbf{f}. \tag{2}$$

Pressure gradient and diffusion terms in the right side of the Navier–Stokes equation are calculated using the particle interaction models developed in the MPS method. For the calculation of pressure, a new incompressibility model using velocity divergence is developed. The left side of Equation (2) shows convection of a fluid in Eulerian co-ordinates. A higher-order convection scheme using a flow directional local grid is presented for the calculation of convection.

3. NUMERICAL METHODS

3.1. MPS models

In the MPS method a particle interacts with others in its vicinity covered with a weight function $w(r)$, where r is the distance between two particles. In this study, the following function is employed

$$w(r) = \begin{cases} -(2r/r_e)^2 + 2 & (0 \le r < 0.5r_e) \\ (2r/r_e - 2)^2 & (0.5r_e \le r < r_e). \\ 0 & (r_e \le r) \end{cases} \tag{3}$$

Since the area that is covered with this weight function is bounded, a particle interacts with a finite number of neighbouring particles. The radius of the interaction area is determined by a parameter r_e. Then the particle number density at a co-ordinate $\mathbf{r}_i$ is defined by

$$\langle n \rangle_i = \sum_j w(|\mathbf{r}_j - \mathbf{r}_i|). \tag{4}$$

Assuming that the particles have the same mass m, the fluid density is proportional to the particle number density:

$$\langle \rho \rangle_i = \frac{m\langle n \rangle_i}{\int_V w(r)\,\mathrm{d}v}. \tag{5}$$

A gradient vector between two particles i and j possessing scaler quantities ϕ_i and ϕ_j at co-ordinates $\mathbf{r}_i$ and $\mathbf{r}_j$ is simply defined by $(\phi_j - \phi_i)(\mathbf{r}_j - \mathbf{r}_i)/|\mathbf{r}_j - \mathbf{r}_i|^2$. The gradient vector at the particle i is given as the weighted average of these gradient vectors:

$$\langle \nabla\phi \rangle_i = \frac{d}{n^0} \sum_{j \ne i} \left[\frac{\phi_j - \phi_i}{|\mathbf{r}_j - \mathbf{r}_i|^2} (\mathbf{r}_j - \mathbf{r}_i) w(|\mathbf{r}_j - \mathbf{r}_i|) \right], \tag{6}$$

where d is the number of space dimensions and n^0 is the particle number density. This model is not sensitive to absolute pressure. This is consistent with the property of incompressible fluids, which only depend on the relative pressure distribution.

Laplacian is an operator representing diffusion. In the MPS method, diffusion is modelled by distribution of a quantity from a particle to its neighbouring particles by use of the weight function:

$$\langle \nabla^2\phi \rangle_i = \frac{2d}{\lambda n^0} \sum_{j \ne i} [(\phi_j - \phi_i) w(|\mathbf{r}_j - \mathbf{r}_i|)], \tag{7}$$

where λ is a parameter by which the variance increase is equal to that of the analytical solution:

$$\lambda = \frac{\int_V w(r) r^2\,\mathrm{d}v}{\int_V w(r)\,\mathrm{d}v}. \tag{8}$$

When the space is two dimensions and Equation (3) is employed as the weight function, the parameter λ is

$$\lambda = \frac{31}{140} r_e^2. \tag{9}$$

This Laplacian model is conservative since the quantity lost by the particle i is just obtained by the particle j.

3.2. Incompressibility model

Generally the continuity equation for incompressible fluid can be written as follows:

$$\frac{D\rho}{Dt} = -\rho(\nabla\cdot\mathbf{u}) = 0. \tag{10}$$

In the MPS method, $D\rho/Dt = 0$ is used for the incompressibility model where the particle number density keeps a constant value of n^0. When the calculated particle number density n^* is not n^0, it is implicitly corrected to n^0. In this model, the particle number density must be proportional to the fluid density, i.e. all the particles should have the same mass. Thus, the local concentration of particles is not allowed.

However, in some situations the concentration of particles is required, for instance, near the boundary. In addition, the particle number density does not change in Eulerian co-ordinates. By using $-\rho(\nabla\cdot\mathbf{u}) = 0$ in Equation (10), these difficulties can be eliminated. As in the same way of the gradient model, the velocity divergence between two particles i and j is defined by $(\mathbf{u}_j - \mathbf{u}_i)\cdot(\mathbf{r}_j - \mathbf{r}_i)/|\mathbf{r}_j - \mathbf{r}_i|^2$. Then the velocity divergence at the particle i is given by the following equation (Figure 1)

$$\langle\nabla\cdot\mathbf{u}\rangle = \frac{d}{n^0}\sum_{j\neq i}\frac{(\mathbf{u}_j - \mathbf{u}_i)\cdot(\mathbf{r}_j - \mathbf{r}_i)}{|\mathbf{r}_j - \mathbf{r}_i|^2}\, w(|\mathbf{r}_j - \mathbf{r}_i|). \tag{11}$$

From Equations (2) and (10) pressure is calculated implicitly:

$$\frac{\mathbf{u}_i^{**} - \mathbf{u}_i^*}{\Delta t} = -\frac{1}{\rho}\langle\nabla P^{n+1}\rangle_i, \tag{12}$$

$$\langle\nabla^2 P^{n+1}\rangle_i = \frac{\rho}{\Delta t}\langle\nabla\cdot\mathbf{u}^*\rangle_i, \tag{13}$$

where u_i^* is the temporal velocity obtained from the explicit calculation and u_i^{**} is the new-time velocity. The right side of Equation (13) is the velocity divergence, which is calculated using Equation (11). The left side of Equation (13) is calculated using the Laplacian model shown in Equation (7). Then one has simultaneous equations expressed by a linear symmetric matrix. These are solved by the incomplete Cholesky conjugate gradient (ICCG)

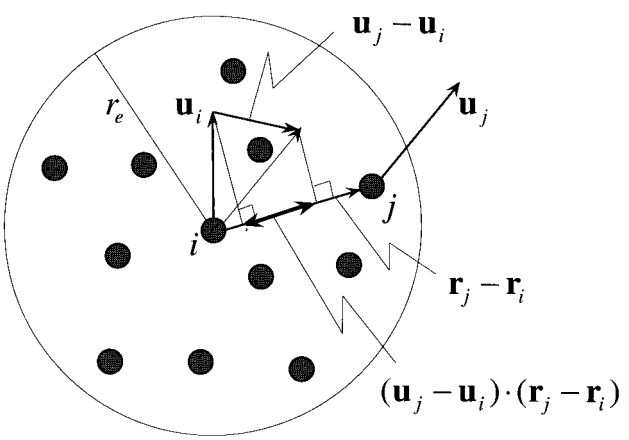

Figure 1. Concept of divergence model.

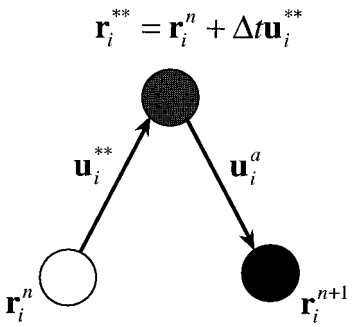

Figure 2. Movement of a particle for the particle–gridless hybrid method.

method. After the pressure calculation, the new-time velocity u_i^{**} is calculated from Equation (12). The gradient model of Equation (6) is applied to the right side of Equation (12). Since this incompressibility model is based on the velocity divergence, the particle number density is allowed to vary and more particles can be placed locally when detailed analysis is needed.

3.3. A higher-order gridless convection scheme

As long as the fluid is isolated from the outside, it can be analysed successfully using the MPS method without solving the convection terms. However, in the problems where inlet and outlet boundaries exist, it is difficult to trace a particle in Lagrangian co-ordinates. In these problems, Eulerian co-ordinates are used and the convection terms are solved explicitly.

The Lagrangian and Eulerian calculations are combined using the concept of the CAT method, where a solution of a convection equation is substituted by $f(t + \Delta t, \mathbf{r}) = f(t, \mathbf{r} - \Delta t \mathbf{u})$. First, a particle located at $\mathbf{r}_i^n$ moves to a new position $\mathbf{r}_i^{**}$ using the velocity $\mathbf{u}_i^{**}$ obtained from the Lagrangian calculation by a particle method. Then, the new-time properties at $\mathbf{r}_i^{n+1}$ are calculated by

$$f(t + \Delta t, \mathbf{r}_i^{n+1}) = f(t, \mathbf{r}_i^{**} - \Delta t \mathbf{u}_i^a). \tag{14}$$

By using an arbitrary convection velocity $\mathbf{u}_i^a$ that can be different from the fluid velocity $\mathbf{u}_i^{**}$, new-time properties at an arbitrary point (computing point) $\mathbf{r}_i^a$ can be interpolated (Figure 2). Depending on the velocity $\mathbf{u}_i^a$, an arbitrary Lagrangian–Eulerian calculation is possible between the fully Eulerian ($\mathbf{u}_i^a = \mathbf{u}_i^{**}$) and the fully Lagrangian ($\mathbf{u}_i^a = 0$) calculations.

In this section an accurate and stable convection scheme is presented for the particle–gridless hybrid method. This scheme consists of four stages as discussed in the following.

3.3.1. Generation of flow directional local grid. In convection, a fluid property is changed along the streamline. Thus, any multi-dimensional convection problem can be regarded as a one-dimensional problem if a computational grid is generated along the flow direction. Considering the flow direction of each computing point (particle), a one-dimensional local grid is generated as shown in Figure 3. Locations and the number of local grid points are determined based on the difference scheme which will be applied to. In this study, two upstream and one downstream grid points are added for the QUICK [17] scheme.

3.3.2. Local interpolation. For the three local grid points on the one-dimensional local grid, the physical properties are interpolated from those of neighbouring particles. A physical property of f_i is calculated from the surrounding discrete values, f_j, as in the same way of MPS or SPH.

$$f_i = \frac{\sum_j f_j w(|\mathbf{r}_j - \mathbf{r}_i|)}{\sum_j w(|\mathbf{r}_j - \mathbf{r}_i|)}. \tag{15}$$

Equation (3) is utilised as the weight function in Equation (15). The interpolation region is limited by a circle (sphere for three dimension) of radius r_e and the lines vertical to the flow direction (Figure 3). If all the particles in r_e distance are used, the interpolation region overlaps for adjacent local grid points and this causes more numerical diffusion.

3.3.3. Convection scheme. Any higher-order difference scheme can be applied easily since a one-dimensional grid has been obtained along the flow direction. A second-order upwind scheme QUICK is applied to those four grid points shown in Figure 3:

$$\tilde{f}_i^{n+1} = f_i^n - q\left(\frac{1}{8}f_{i-2}^n - \frac{7}{8}f_{i-1}^n + \frac{3}{8}f_i^n + \frac{3}{8}f_{i+1}^n\right), \tag{16}$$

$$q = \frac{(u^2 + v^2)^{1/2}\Delta t}{\Delta r}, \tag{17}$$

where Δr is the distance between the local grid points.

3.3.4. MMT filtering. Usually a higher-order scheme results in oscillatory solutions. To prevent the overshoot and undershoot in the solution obtained in the third stage, a filtering scheme MMT is applied. Maximum and minimum limits are calculated at each time step and the solution of a higher-order calculation is bounded by them.

$$f_i^{n+1} = \begin{cases} \tilde{f}_i^{n+1} & \min(f_i^n) \le \tilde{f}_i^{n+1} \le \max(f_i^n) \\ \min(f_i^n) & \tilde{f}_i^{n+1} < \min(f_i^n) \\ \max(f_i^n) & \tilde{f}_i^{n+1} > \max(f_i^n) \end{cases}. \tag{18}$$

Here $\min(f_i^n)$ and $\max(f_i^n)$ are calculated within the one-dimensional local grid.

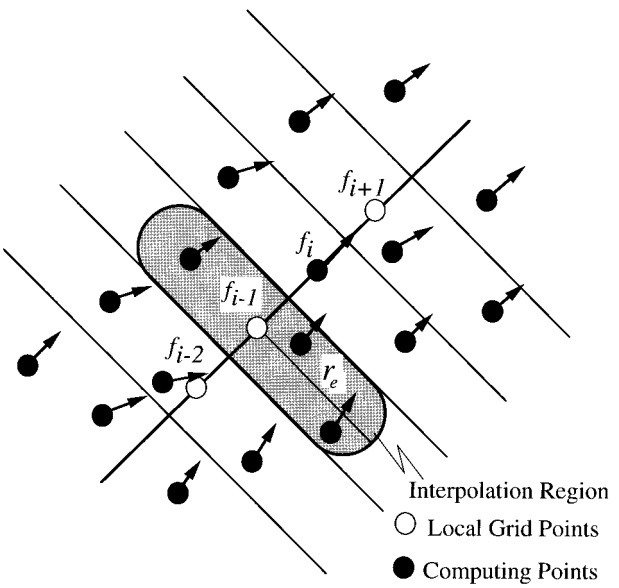

Figure 3. Generation of flow directional local grid.

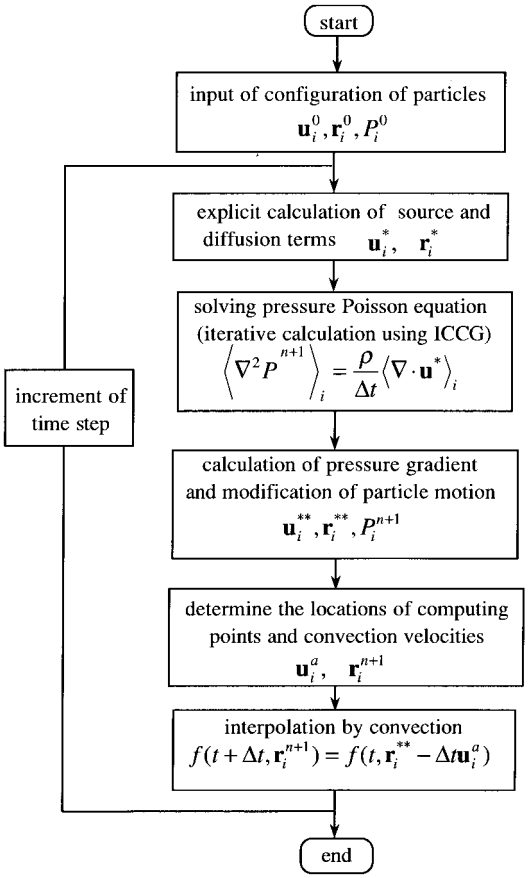

Figure 4. Calculation algorithm of the particle–gridless hybrid method.

The overall algorithm of the particle–gridless hybrid method is shown in Figure 4. In each time step, source and diffusion terms are explicitly calculated, and temporal velocities $\mathbf{u}^*$ and co-ordinate $\mathbf{r}^*$ are obtained. The Poisson equation of pressure is solved with the source term representing the velocity divergence, and then co-ordinates and velocities are corrected to $\mathbf{r}^{**}$ and $\mathbf{u}^{**}$. After the Lagrangian calculation, a new particle positions $\mathbf{r}^{n+1}$ and convection velocities $\mathbf{u}^a$ are determined. Finally, one has new-time properties using the convection scheme.

3.4. Boundary conditions

In a gridless method, an interpolated quantity at boundary $\langle f \rangle_{b.c.}$ does not coincide with the exact value $f_{b.c.}$. When a strict condition is needed at the boundary, a set of simultaneous equations have to be solved for the quantities at the particles beyond the boundary. Instead of solving a matrix, boundary values are assigned explicitly to the particles beyond the boundary so that the interpolated value $\langle f \rangle_{b.c.}$ approximate $f_{b.c.}$. For example, in a free-slip condition, the velocity of an outside particle that is parallel to the wall is equal to that of the nearest inner particle. In a no-slip condition, the velocity distribution of the outside particles are given to be opposite to that of the inner particles. The Neumann boundary condition is applied to the

implicit calculation of pressure Poisson equation. This pressure boundary condition is easily implemented through the Laplacian model in Equation (7). If there is N inside particles, one has N simultaneous linear equations expressed by an $N \times N$ symmetric matrix where the coefficients of the matrix are given by Equation (7). The Neumann boundary condition is satisfied if the pressure of a particle j beyond the boundary equals that of the boundary particles, i.e. $P_j = P_i$. This may be approximated by an alternative expression of Equation (7).

$$\langle \nabla^2 P \rangle_i = \frac{2d}{\lambda n^0} \sum_{\substack{j \neq i \\ j \neq out}} (P_j - P_i) w(|r_j - r_i|). \tag{7a}$$

4. TEST CALCULATION

4.1. Two-dimensional convection problem

The accuracy and the stability of the present convection scheme is examined in a two-dimensional problem of pure convection. A time-dependent two-dimensional convection equation for this test calculation is expressed as follows:

$$\frac{\partial f}{\partial t} + u \frac{\partial f}{\partial x} + v \frac{\partial f}{\partial y} = 0. \tag{19}$$

Figure 5 shows the initial profile of a square wave that rotates anti-clockwise with an angular velocity $\omega = \pi/5$. One revolution of the square wave is simulated using 10^4 particles. Particle distribution is assumed uniform or random.

Time step Δt is limited by the Courant condition just like in the conventional difference scheme. For instance, in a convective calculation, Δt is determined by $\Delta t \leq \Delta r_{\text{avg}}/u$ where Δr_{avg} is the average particle distance. In this study, Δt is fixed at 0.005 for all cases. Both r_e and Δr are assumed as 1.5 times of the average distance between adjacent particles. The optimum

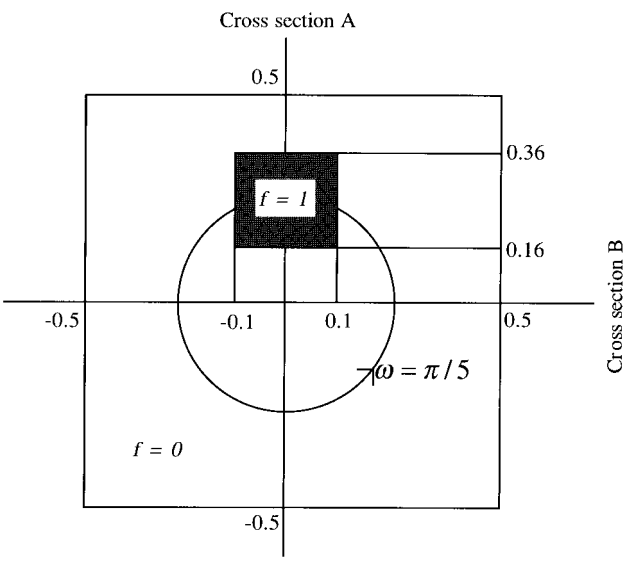

Figure 5. Test problem.

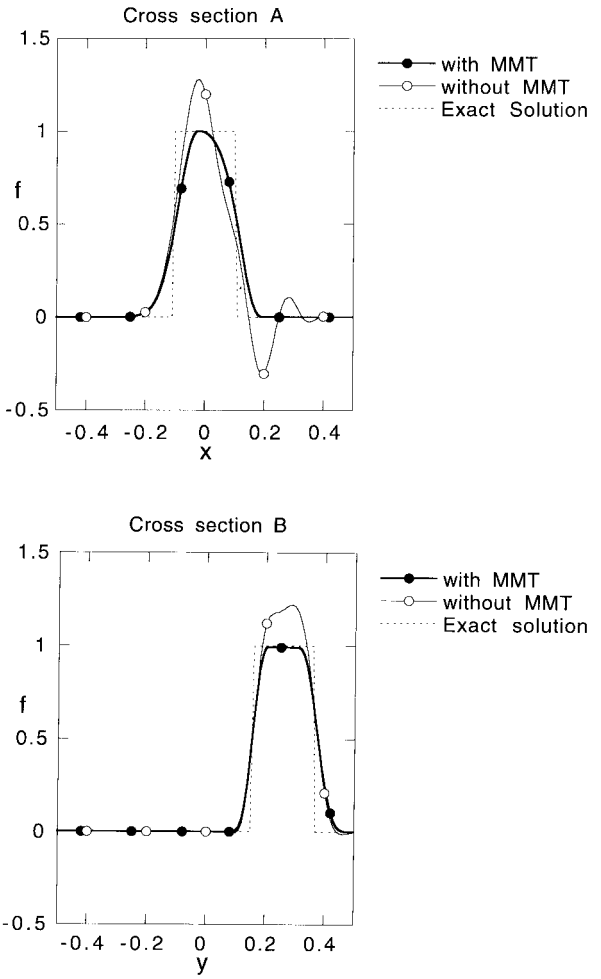

Figure 6. Comparison of the results with and without filter.

values of r_e and Δr are investigated in the next section. In this calculation the artificial convection velocity $\mathbf{u}_i^a$ in Equation (14) is equal to the velocity of flow $\mathbf{u}_i^{**}$ for a pure Eulerian calculation.

Figure 6 shows the profile after one revolution predicted by the present scheme with and without the MMT filter. The overshoot and undershoot are large in a cross-section A without the filter. However, the overshoot and undershoot have been successfully removed after the MMT filtration. Figure 7 show the profiles predicted by the present scheme, CAT and the least-square method with uniform particle distribution. The profile predicted by the least-square method is broadened due to the excessive numerical diffusion. Accurate profiles are obtained in the calculations with the present scheme and the CAT method and more stable solution is obtained with the present scheme. Figure 8 shows the comparison with random particle distribution. The particle distribution is obtained by distorting the uniform distribution slightly. When the particle distribution is highly random, calculation with the CAT method fails due to the bad-shaped triangles. Compared with the uniform distribution case, the present scheme shows more accurate and stable results than the others.

4.2. Optimum radius of weight function and local grid size

The radius of weight function r_e and local grid size Δr are important parameters for interpolation. When r_e is small, numerical instability occurs since there is not enough particles for interpolation. A large r_e results in inaccurate solutions and a longer computation is needed for interpolation. The smallest r_e that does not cause numerical instability is chosen as an optimum value. It is not necessary to use a common value of r_e for each calculation model, gradient model in Equation (6), divergence model in Equation (11), Laplacian model in Equation (7) and local interpolation in Equation (15). In a previous study [7], it had been already optimised for gradient and Laplacian models as 2.0 and 4.0 times of average particle distance Δr_{avg} respectively. The same value of r_e that is employed in the gradient model is used for divergence calculations since the formulations are similar to each other. To optimise the radius of weight function r_e and the local grid size Δr, sensitivity analysis is carried out with respect to r_e and Δr for random particle distribution. The two-dimensional convection problem in Equation (19) is calculated with various r_e and Δr. Figure 9 shows the mean square errors of each calculation. When r_e is smaller than $1.3\,\Delta r_{\text{avg}}$, the neighbouring particles are so small

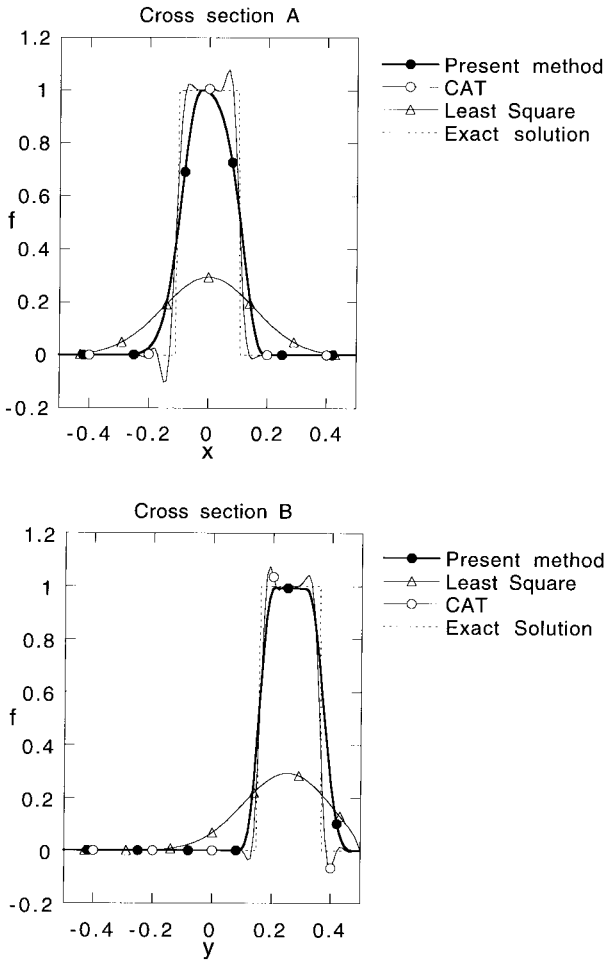

Figure 7. Comparison of various gridless methods (uniform).

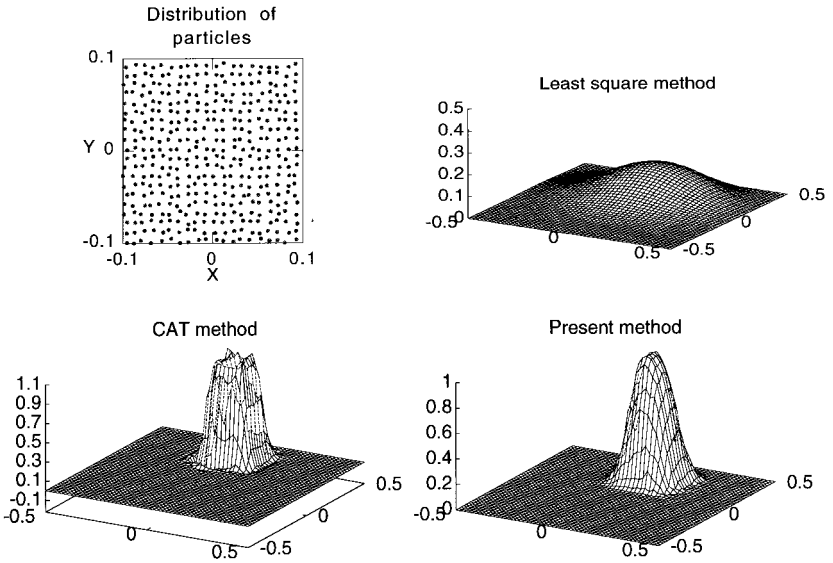

Figure 8. Comparison of various gridless methods (random).

that numerical instability occurs. The error grows as r_e becomes large. $r_e = 1.5\,\Delta r_{\text{avg}}$ is chosen for the present study as the smallest value that does not cause the numerical instability. With respect to the local grid size Δr, the error becomes small when Δr is between $1.5\,\Delta r_{\text{avg}}$ and $2.5\,\Delta r_{\text{avg}}$. In this study, $1.5\,\Delta r_{\text{avg}}$ is used for Δr in accordance with r_e.

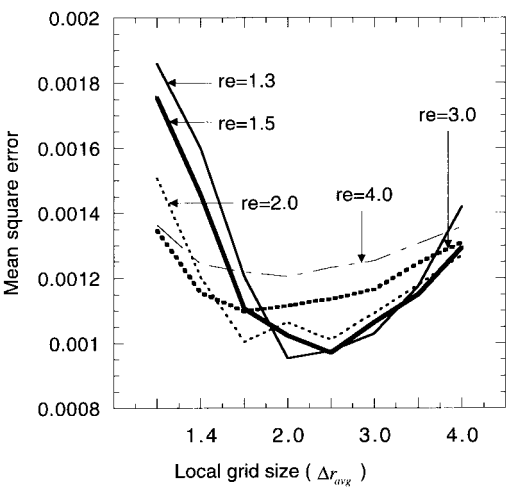

Figure 9. Effect of r_e and local grid size in local interpolation.

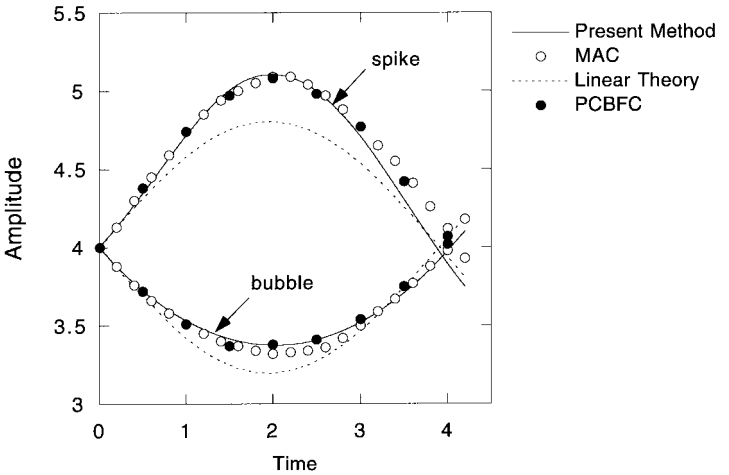

Figure 10. Amplitude of spike and bubble.

5. ANALYSIS OF INCOMPRESSIBLE FLOW WITH A FREE-SURFACE

5.1. Sloshing initiated by a pressure spike

The first example is chosen to show that the present method can simulate the oscillatory free-surface motion initiated by external excitation. A two-dimensional rectangular vessel of the width of 4.8 units is filled with liquid to the height of 4.0 units. The fluid has the unit density and the viscosity of 0.01. Surface tension is not specified. The unit gravity acceleration works downwards. A pressure spike of the cosine profile of the unit strength initiates the oscillation of free-surface. This benchmark problem was first proposed by Harlow and Welch, who analysed the problem with the marker-and-cell (MAC) [18] method. Ramaswamy and Kawahara [19] calculated the problem with the Lagrangian finite element method. Recently, the problem was analysed by Takizawa *et al.* with the physical component boundary fitted co-ordinate (PCBFC) [15] method using 120 cells with the central difference scheme. In the present work, the problem is analysed with the particle–gridless hybrid method using 1043 computing points. Free-slip conditions are imposed on the wall particles. To avoid the numerical drag on the wall, the left and right wall particles are moved depending on the free-surface level. After the Lagrangian phase, particle positions are redistributed so that only the vertical co-ordinates are changed with respect to the elevation of the free-surface.

The accuracy of the gradient and the divergence models in Equations (6) and (11) respectively, are dependent upon the particle distribution. This is illustrated in the following equation, where Equation (6) is expanded using a Taylor series for the one-dimensional case.

$$\mathrm{Err} = \left\langle \frac{\partial f}{\partial x} \right\rangle_i - \left. \frac{\partial f}{\partial x} \right|_i = \frac{1}{2n_i} \left. \frac{\partial^2 f}{\partial x^2} \right|_i \sum_{i\,j \neq i} (x_j - x_i) w_{ji} + \frac{1}{6n_i} \left. \frac{\partial^3 f}{\partial x^3} \right|_i \sum_{i\,j \neq i} (x_j - x_i)^2 w_{ji} + \cdots \tag{20}$$

In Equation (20), the first-order term in the right-hand-side becomes large near the free-surface where the particles are distributed asymmetrically. To reduce the error on the free-surface, one additional layer of 'ghost' particles are located above the free-surface for the calculation of pressure gradient.

Amplitudes of a spike (higher end) and a bubble (lower end) of the free-surface in its half period are shown in Figure 10 with those obtained by the linear theory, the MAC method and

the PCBFC method. Both the amplitude and the period of sloshing estimated by the present method agree well with the results by the MAC and the PCBFC methods. Computed free-surfaces and flows up to 8 s are shown in Figure 11. It shows curved free-surfaces formed by non-linear effects of flow.

5.2. Flow-induced sloshing in a thin rectangular tank

For the application of the present method to a problem that has the inlet and outlet flows, a flow-induced sloshing is analysed. Flow-induced sloshing is one of the important phenomena for the safety design of liquid metal cooled fast breeder reactors (LMFBRs) to assure stable flow of the coolant. Okamoto and Madarame [20] performed an experimental investigation of flow-induced sloshing with various tank geometries. Three flow states were observed in the

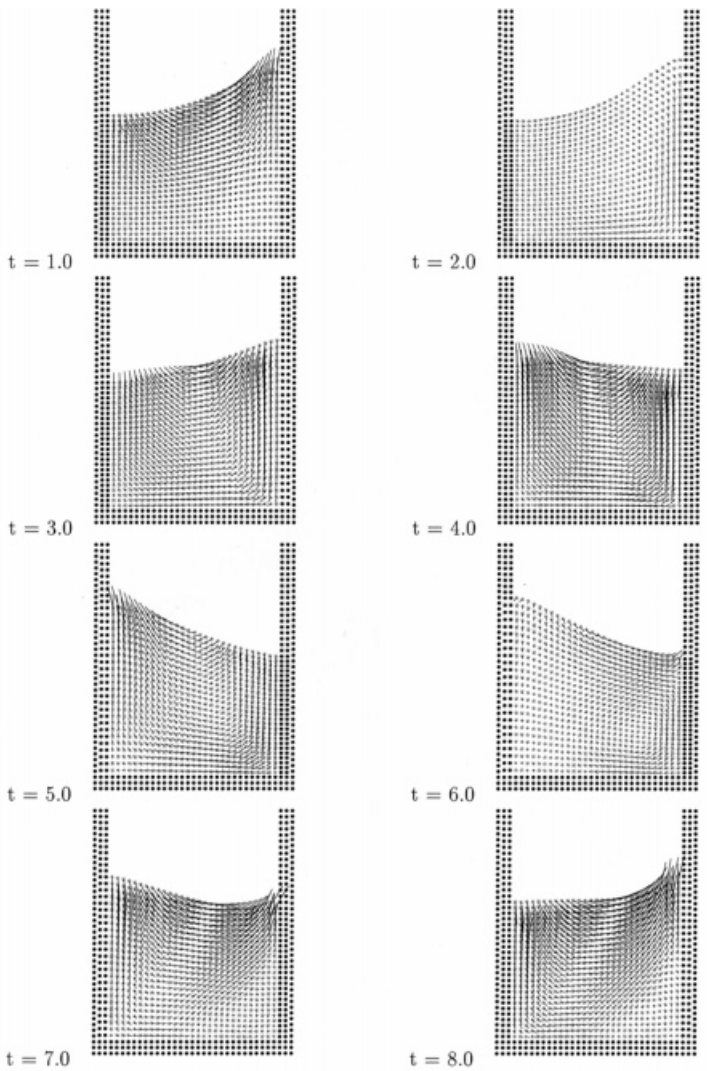

Figure 11. Free-surface motions and the inside flows initiated by a pressure spike.

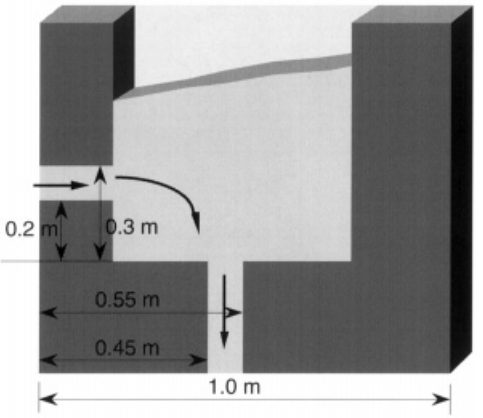

Figure 12. Schematic apparatus of test section.

experiment, i.e. stable state, oscillating state and reverse flow pattern state. In the stable state, the free-surface and the flow pattern are stable and unique. The main vortex flows in the counter-clockwise direction with a small vortex at the left bottom corner. Oscillating states were observed in some geometries, where the free-surfaces periodically oscillate with a certain amplitude. In the reverse flow pattern state, only one vortex existed in clockwise direction. Among the various tank geometries, one geometry has been chosen for this study, where the flow-induced oscillation was observed. It is a two-dimensional rectangular tank with a width of 1.0 m and a thickness of 0.1 m. An inlet duct of the width 0.1 m was connected horizontally at the left wall of the tank at the height of 0.2–0.3 m from the bottom. An outlet duct of the width of 0.1 m is connected at the centre of the bottom. Figure 12 shows a schematic apparatus of the experimental section. Water is injected with the constant velocity, and the water level is controlled by an overflow tank.

Numerical simulations were performed using the BFC [15] and PCBFC [16] methods. In the simulation using the PCBFC method, the free-surface oscillated under a certain water level and inlet velocity conditions. The secondary flow caused the surface potential variation. The oscillation energy was assumed to be transferred from the kinetic energy of forced circulation by a non-linear wave created by the secondary flow. By the BFC method, the mechanism of the oscillation was quantitatively investigated. The sloshing was considered to depend on the interaction between the flow and the free-surface. However, in these methods, calculations failed when the injection velocity was high due to the large deformation of the free-surface.

This experiment is analysed by the particle–gridless hybrid method with several injection velocities and water levels. Velocity is given at the inlet and outlet, and free-slip conditions are imposed to the walls to avoid the excessive drag. The number of fluid particles varies from 1018 to 1213 depending on the initial water level, which varies from 0.4 to 0.65 m. Injection velocities are varied from 0.5 to 1.2 $\mathrm{m\,s^{-1}}$. The kinematic viscosity is given about 100 times larger than the value of water in order to account the effect of turbulent viscosity. The time step is fixed to be 0.005 s.

Figure 13 compares the range of the occurrence of sloshing predicted by present method with the experimental data in terms of injection velocity and average water level. In these maps the stable regions where sloshing does not occur is denoted by cross ($\times$). The experimental data show that the sloshing has occurred when the injection velocity is between 0.6 and 1.1 $\mathrm{m\,s^{-1}}$. The sloshing is more likely to occur when the water level is relatively low. The BFC

method [15] failed the calculation when the inlet velocity is larger than 0.7 m s^{-1} with the water level below 0.45 m. This was due to the large deformation of the free-surface. The present method predicts the occurrence of sloshing fairly good and the simulations proceeded successfully even with higher injection velocities.

Figure 14 show the computed shapes of free-surfaces and flows of the sloshing at every 0.2 s starting at 24 s when the injection velocity is 1.1 m s^{-1} and the average water level is 0.5 m.

6. CONCLUSIONS

The particle–gridless hybrid method for analysing incompressible flow has been developed. The method consists of Lagrangian and Eulerian calculations. For the Eulerian calculation, a higher-order convection scheme is developed based on a flow directional local grid. It can be applied to multi-dimensional problems easily since it is based on a one-dimensional local grid. This scheme is verified for a two-dimensional pure convection problem with uniform and random particle distributions and the results show that the present scheme is more accurate and stable than the other methods. For the Lagrangian phase, a new incompressibility model using velocity divergence is proposed. The pressure gradient model and the diffusion model developed in MPS method is used.

The present method is first applied to the analysis of sloshing induced by a external pressure spike. Both the amplitude and the period of sloshing agree well with the results calculated by the MAC and BFC methods. As an application to a problem that has an inlet and an outlet, sloshing induced by injected flow is analysed. Occurrence of sloshing is investigated in terms of the injection velocity and the average water level. The range of the occurrence is nearly the same with that of the experiment. The analysis is successful using the present method even if the inlet velocity is more than 1.0 m s^{-1}.

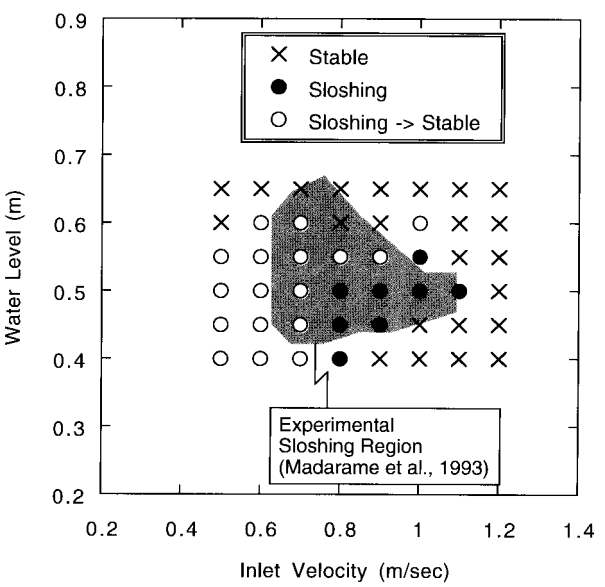

Figure 13. Sloshing map estimated by the present method.

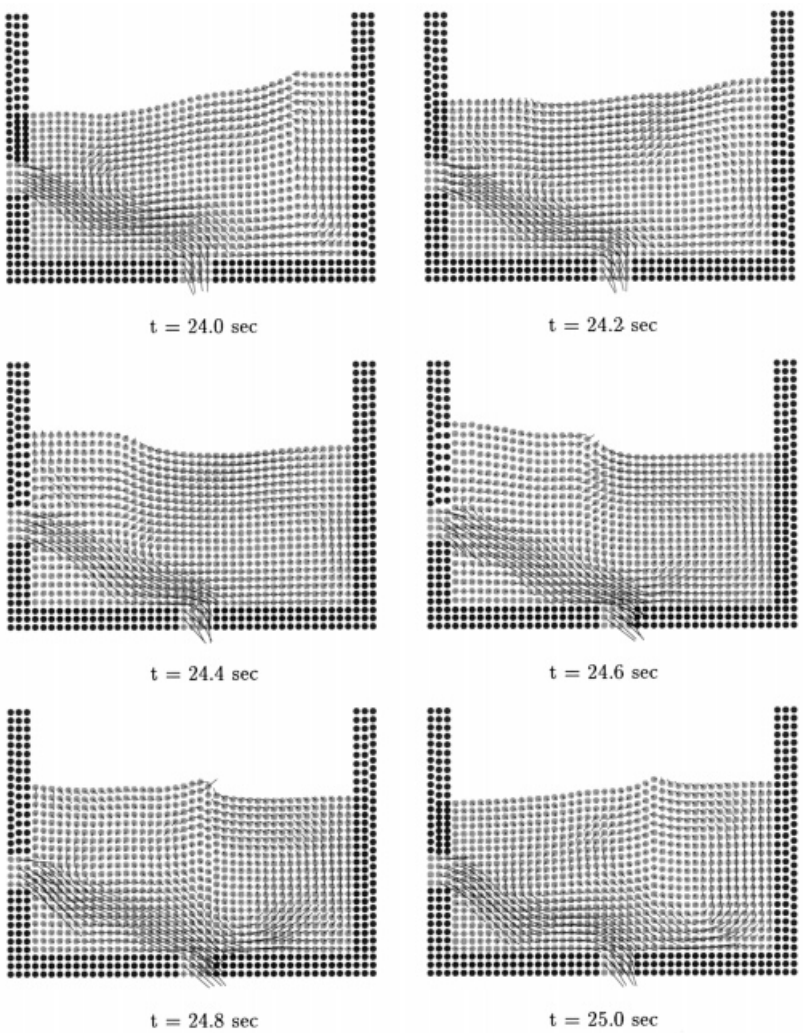

Figure 14. Sloshing free-surfaces and flows.

REFERENCES

1. J.J. Monaghan, 'An introduction to SPH', *Comput. Phys. Commun.*, **48**, 89 (1988).
2. W. Benz, 'Smoothed particle hydrodynamics: a review', *The Numerical Modeling of Nonlinear Stellar Pulsations—Problems and Prospects*, Kluwer Academic, Norwell MA, 1989, p. 269.
3. S. Koshizuka, H. Tamako and Y. Oka, 'A particle method for incompressible viscous flow with fluid fragmentation', *Comput. Fluid Dynam. J.*, **4**, 29–46 (1995).
4. S. Koshizuka, H. Ikeda and Y. Oka, 'Numerical simulation of fragmentation processes in vapor explosions using moving particle semi-implicit method', *Proc. Int. Meeting on Advanced Reactors Safety*, Florida, June 1–5, 1997, pp. 872–879.
5. T. Batina, 'A gridless Euler/Navier–Stokes solution algorithm for complex aircraft applications', *AIAA Paper 93–0333*, American Institute of Aeronautics and Astronautics, 1993.
6. T. Belytschko Y.Y. Lu and L. Gu, 'Element free Galerkin methods', *Int. J. Numer. Methods Eng.*, **37**, 229 (1994).
7. S. Koshizuka and Y. Oka, 'Moving-particle semi-implicit method for fragmentation of incompressible fluid', *Nucl. Sci. Eng.*, **123**, 421–434 (1996).
8. S. Koshizuka and Y. Oka, 'Development of a particle method for calculating fragmentation of incompressible viscous fluid', *Proc. US–Japan Joint Seminar: A Multidisciplinary International Seminar on Intense Multiphase Interactions*, Santa Barbara, June 9–13, 1995, pp. 145–158.

9. N. Tanaka, 'High accuracy gridless algorithm and the application to particle methods', *Proc. JSCES Conference on Computational Engineering and Science*, No. 1-1, May 1996, pp. 7–10. (in Japanese)
10. T. Yabe and T. Aoki, 'A universal solver for hyperbolic equations by cubic-polynomial interpolation', *Comput. Phys. Commun.*, **66**, 219 (1991).
11. C.W. Hirt, A.A. Amsden and J.L. Cook, 'An arbitrary Lagrangian–Eulerian computing method for all flow speeds', *J. Comput. Phys.*, **14**, 227–253 (1974).
12. S. Koshizuka, C.B. Carrico, S.W. Lomperski, Y. Oka and Y. Togo, 'Min–max truncation: an accurate and stable filtering method for difference calculation of convection', *Comput. Mech.*, **6**, 65 (1990).
13. J.E. Welch, F.H. Harlow, J.P. Sharmon and B.J. Daly, 'The MAC method', *LA-3425*, 1966.
14. D. Nichols, C.W. Hirt and R.S. Hotchkiss, 'SOLA-VOF, a solution algorithm for transient fluid flows with multiple free boundaries', *LA-8355*, 1980.
15. S. Saeki, H. Madarame, K. Okamoto and N. Tanaka, 'Numerical study on the self-induced sloshing', *ASME Fluids Engineering Division Summer Meeting*, *FEDSM97-3401*, June 22–26, 1997.
16. A. Takizawa, S. Koshizuka and S. Kondo, 'Generalization of physical components boundary fitted co-ordinate (PCBFC) method for the analysis of free-surface flow', *Int. J. Numer. Methods Fluids*, **15**, 1213–1237 (1992).
17. B.P. Leonard, 'A stable and accurate convective modelling procedure based on quadratic upstream interpolation', *Comp. Methods Appl. Mech. Eng.*, **19**, 59–98 (1979).
18. F.H. Harlow and J.E. Welch, 'Numerical study of large-amplitude free-surface motions', *Phys. Fluids*, **9**, 842–851 (1966).
19. B. Ramaswamy and M. Kawahara, 'Lagrangian finite element analysis applied to viscous free surface fluid flow', *Int. J. Numer. Methods Fluids*, **7**, 953–984 (1987).
20. K. Okamoto, H. Madarame and M. Fukaya, 'Flow pattern and self-induced oscillation in a thin rectangular tank with free surface', *J. Faculty Eng.*, The University of Tokyo, **XLII**, 123–142 (1993).

